# DIAGNOSTICS OF A HYDROCARBON PLASMA JET USING THE $A^2\Delta - X^2\Pi$ SYSTEM OF CH

J. KOULIDIATI[a], A. CZERNICHOWSKI[b], J.J. BEULENS[c] AND D.C. SCHRAM[c]

[a]Université de Ouagadougou, Département de Physique
B.P. 7021 Ouagadougou 03, Burkina Faso
[b]Université d'Orléans, Faculté des Sciences, B.P. 6759, 45067 Orléans Cedex 2, France
[c]Eindhoven University of Technology
P.O. Box 513, 5600 MB Eindhoven, The Netherlands

*(Received January 27, 1998; revised version June 29, 1998)*

We study the intensity distribution of the $A^2\Delta - X^2\Pi$ system of CH molecule at 430 nm in a low pressure plasma jet. This system shows an overlap of vibrational bands with $\Delta v = 0$. By comparing simulated and experimental emission spectra, we obtain rotational and vibrational temperatures using Boltzmann plots or some thermometer functions. The thermometer functions are the integrated intensities of line-like transitions composed of several rotational transitions. The result of the Boltzmann plots and the thermometer functions method that we propose are in good agreement.

PACS numbers: 07.20.Dt, 52.70.Kz, 33.20.–t

## 1. Introduction

Applications of low temperature plasmas are of great importance: treatment of exhaust gases [1], thin film deposition (a-C:H, diamond, graphite) [2, 3], hydrocarbon processing [4], and others. These plasmas present deviations from the thermal equilibrium, and consequently, elaborate spectroscopic analyses are difficult to perform. Mostly, a high performance spectroscopic equipment is needed. In this paper, the proposed method shows a good potential to be used as a simple diagnostics. We use it for measuring temperatures in a low pressure hydrocarbon plasma jet showing a small deviation from thermal equilibrium with temperatures between 1000 and 6000 K.

## 2. Experimental set-up

The experimental set-up shown in Fig. 1 is used for the preparation of thin films. By varying macroscopic parameters like arc power, gas flow rates (Ar, $C_xH_y$, $H_2$), pressure, etc., deposition of diamond, graphite or amorphous carbon (a-C:H) is possible.

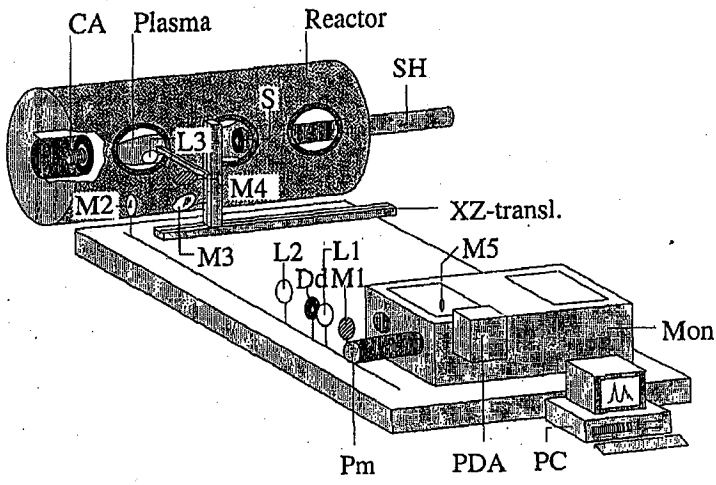


Fig. 1. Experimental set-up: CA: cascade arc, S: substrate, SH: sample holder, L1–L3: lenses, M1–M5: mirrors, Dd: diaphragm, Mon: monochromator, PDA: photo diode array, Pm: photo multiplier, PC: personal computer.

In a wall-stabilised arc (cascade arc of the Maecker type) an argon plasma is created at sub-atmospheric pressure [3] with a current of 20–100 A [5]. After passing a nozzle the plasma expands in a deposition chamber at a significantly lower pressure (10–1000 Pa) [6].

Due to a large pressure drop between the arc and the vessel the plasma expands supersonically in the vacuum chamber. The plasma velocity increases up to 4 km/s before a shock occurs after which the plasma flows subsonically at velocities of 1 km/s [7].

At the anode side a methane flow is injected. It is dissociated and ionised there by the argon arc plasma. The experimental conditions for the spectroscopic study are those used for amorphous carbon films deposition: 100 scc/s Ar flow rate, 4.44 scc/s $CH_4$ flow rate, vessel pressure 100 Pa, and arc current 50 A.

The optical system, described in more detail in Ref. [7], is formed by four mirrors (M1–M4), three lenses (L1–L3), and a diaphragm. This system makes it possible to shift the optical axis in a vertical and a parallel translation with respect to the plasma jet. The plasma is imaged at the entrance slit of a monochromator (Czerny–Turner, 1 m THR 1000 of Jobin–Yvon), with 1200 lines/mm, and a dispersion of 0.8 nm/mm at 500 nm. A Peltier cooled (−14.5°C) photo-diode array (Reticon RL 1024S) consisting of 1025 photo-elements (25 $\mu$m width each) is used as a detector. The system is calibrated using a tungsten ribbon lamp with a known spectral intensity. A spectral region of about 20 nm can be registered in 1024 points. The background spectrum was registered with only argon-fed arc, at the same other operational conditions. It gives us a zero-line by a point-by-point subtraction of some weak Ar lines present at the examined spectral range so that the proper signal for further numerical processing can be established.

## 3. Results

The experimental setting for amorphous carbon deposition are used. In Fig. 2, both experimental and simulated spectra of the $A^2\Delta - X^2\Pi$ transition of CH are superposed.

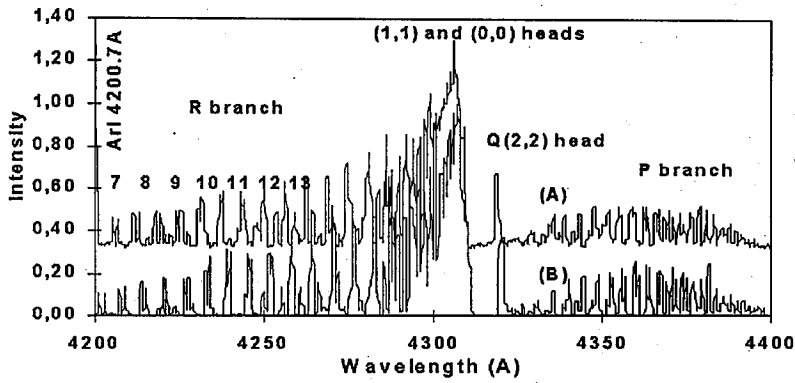


Fig. 2. Superposition of experimental (A) ([Ar] = 100 scc/s, [$CH_4$] = 4.44 scc/s, $p$ = 100 Pa, $I_{arc}$ = 50 A) and simulated (B) spectrum ($T_V$ = 3100 K, $T_R$ = 3000 K) of CH.

The relative intensity of a rotational transition is given by

$$I(v'v''N'N'') = \frac{f_{v'v''}}{f_{00}}\sigma^4 S_{N'N''} \exp\left[\frac{-hcG(v)}{kT_V}\right] \exp\left[\frac{-hcF'(N)}{kT_R}\right], \tag{1}$$

where we use the habitual spectroscopic notation; $f_{v'v''}$ takes into account the Franck–Condon factors $q_{v'v''}$, $f_{00}$ is relative to the (0,0) band, $G(v)$ is the energy of the vibrational level given by

$$G(v) = \omega_e\left(v+\frac{1}{2}\right) - \omega_e x_e\left(v+\frac{1}{2}\right)^2, \tag{2}$$

where $\omega_e$ is the vibrational frequency and $\omega_e x_e$ accounts for a deviation of the oscillator from a harmonic oscillator, $S_{N'N''}$ is the line strength (Hönl–London factor) [8], $F'(N)$ is the energy of the rotational level of the $A^2\Delta$, $T_V$ is the vibrational temperature and $T_R$ is the rotational temperature. In the case of doublet states, each rotational level is divided into two principal energy levels; for the $^2\Pi$ state, each level splits in two sub-levels (noted $c$ and $d$); this is called the $\Lambda$-type doubling. The energetic terms corresponding to the two groups of principal levels are given by

$$F_1(N) = T_1(N) + S(N) \pm \frac{1}{2}\Delta\nu_{cd}(N) + K(N) \tag{3a}$$

$$F_2(N) = T_2(N) + S(N) \pm \frac{1}{2}\Delta\nu_{cd}(N) - K(N) \tag{3b}$$

with $N = J + 1/2$ for $F_1$ and $N = J - 1/2$ for $F_2$. The terms used in formulae (3a) and (3b) are the following:

$$T_{1,2}(J) = B_V J_\Lambda - J_\Lambda^2 - H_V J_\Lambda^3 - 4D_V + 12H_V J_\Lambda$$

$$\pm(1/2)B_V\left[4(J+1/2)^2 C^2(J_\Lambda) + 4Y_V(Y_V - 4C(J_\Lambda))\right]^{1/2}, \tag{4}$$

where

$$J_\Lambda = \left(J + \frac{1}{2}\right)^2 - \Lambda^2 \tag{5a}$$

and

$$C(J_\Lambda) = 1 - 2\frac{D_V}{B_V}J_\Lambda + 3\frac{H_\Lambda}{B_V}J_\Lambda^2. \tag{5b}$$

The value of $\Lambda$ is 2 for the $\Delta$ state and 1 for the $\Pi$ state. The terms

$$S_1(N) = \frac{1}{2}\gamma N \tag{6a}$$

and

$$S_2(N) = \frac{1}{2}\gamma(N+1) \tag{6b}$$

represent the spin doubling. The energetic terms taking into account the $\Lambda$-type doubling in the $^2\Pi$ state are the following:

$$\Delta v_{cd}(N) = q_i N(N+1) - 4v_i N^2(N+1)^2, \qquad i = 1,2 \tag{7}$$

(we neglect the $\Lambda$-type doubling in the $^2\Delta$ state). The term $K(N)$ is given by

$$K(N) = aN^3 + bN^2 + cN + d, \tag{8}$$

where $a = 0.0016980014$, $b = -0.047615718$, $c = 0.46444479$, $d = -0.955203$, are generated by Koulidiati et al. [9] for large rotations because of the errors induced by the constants $q_i$ and $v_i$ that are calculated with the ten first rotational numbers. The molecular constants used in the simulation are taken from Phillips [10] and Herzberg [11, 12]. The procedure of simulation is described in Ref. [13].

The results concerning the calculation of wavelengths are in good accordance with experimental values of Fagerhölm [14] , Gerö [15] and Bembenek et al. [16]. An analysis of the simulated spectrum shows that some spectral lines ($10 < N < 24$) are well isolated and can be therefore used as "thermometric lines". The integrated intensities of these thermometric lines can be deduced from Table I. The method that we propose does not rely on very well-isolated individual spectral lines. The only requirement is to know the exact positions of both red and violet wing limits of the lines. Moreover, they can be simple or complex but it changes nothing because only integrated relative line intensities are needed. Some of these thermometric lines from 420 to 440 nm are shown in Fig. 2.

When plotting a function of $\ln(I(V'V''N'N'')/S_{N'N''})$ versus $F'(N)$ for the rotational levels of the $A^2\Delta$ level the rotational temperature can be deduced as is shown in Fig. 3, where $I(V'V''N'N'')$ is the integrated intensity of the thermometric lines and $S_{N'N''}$ is the sum of the Hönl–London factors of the constituting rotational levels.

TABLE I

Thermometric lines of the $A^2\Delta - X^2\Pi$ system of CH.

| No. | Composition | Vibration band | $\sum S_{N'N''}$ | $\lambda_{\text{center}}$ [nm] | $F'(N)$ [$\text{cm}^{-1}$] | $N(N+1)$ |
|---|---|---|---|---|---|---|
| 1 | R1dc(23)+R2dc(23) | 0– 0 | 37.03 | 417.15 | 7527 | 552 |
| 2 | R1cd(22)+R2cd(22) | 0–0 | 26.03 | 417.40 | 6926 | |
| 3 | R1dc(22)+R2dc(22) | 0–0 | 26.03 | 417.75 | 6926 | 506 |
| 4 | R1cd(21)+R2cd(21) | 0–0 | 25.03 | 418.00 | 6352 | 462 |
| 5 | R1dc(21)+R2dc(21) | 0–0 | 25.03 | 418.30 | 6352 | 462 |
| 6 | R1cd(19)+R2cd(19) | 0–0 | 88.10 | 419.20 | 5260 | 380 |
| | R1dc(24)+R2dc(24) | 1–1 | | | | |
| | R1cd(23)+R2cd(23) | 1–1 | | | | |
| 7 | R1cd(18)+R2cd(18) | 0–0 | 69.12 | 420.10 | 4748 | 342 |
| | R1dc(18)+R2dc(18) | 0–0 | | | | |
| | R1dc(21)+R2dc(21) | 1–1 | | | | |
| 8 | R1cd(16)+R2cd(16) | 0–0 | 62.13 | 421.05 | 3793 | 272 |
| | R1dc(16)+R2dc(16) | 0–0 | | | | |
| | R1cd(18)+R2dc(18) | 1–1 | | | | |
| 9 | R1cd(15)+R2cd(15) | 0–0 | 59.14 | 421.65 | 3351 | 240 |
| | R1dc(15)+R2dc(15) | 0–0 | | | | |
| | R1dc(17)+R2dc(17) | 1–1 | | | | |
| 10 | R1cd(14)+R2cd(14) | 0–0 | 56.15 | 422.30 | 2935 | 210 |
| | R1dc(14)+R2dc(14) | 0–0 | | | | |
| | R1dc(16)+R2dc(16) | 1–1 | | | | |
| 11 | R1cd(13)+R2cd(13) | 0–0 | 52.16 | 422.90 | 2544 | 182 |
| | R1dc(13)+R2dc(13) | 0–0 | | | | |
| | R1cd(14)+R2cd(14) | 1–1 | | | | |
| 12 | R1cd(12)+R2cd(12) | 0–0 | 49.17 | 423.60 | 2178 | 156 |
| | R1dc(12)+R2dc(12) | 0–0 | | | | |
| | R1cd(13)+R2cd(13) | 1–1 | | | | |
| 13 | R1cd(11)+R2cd(11) | 0–0 | 46.18 | 424.40 | 1839 | 132 |
| | R1dc(11)+R2dc(11) | 0–0 | | | | |
| | R1cd(12)+R2cd(12) | 1–1 | | | | |
| 14 | R1cd(10)+R2cd(10) | 0–0 | 43.19 | 424.80 | 1526 | 110 |
| | R1dc(10)+R2dc(10) | 0–0 | | | | |
| | R1cd(11)+R2cd(11) | 1–1 | | | | |

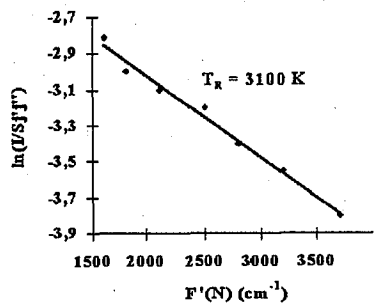


Fig. 3. Boltzmann plot for the $A^2\Delta - X^2\Pi$ system of CH: ([Ar] = 100 scc/s, [$CH_4$] = 4.44 scc/s, $p$ = 100 Pa, $I_{arc}$ = 50 A).

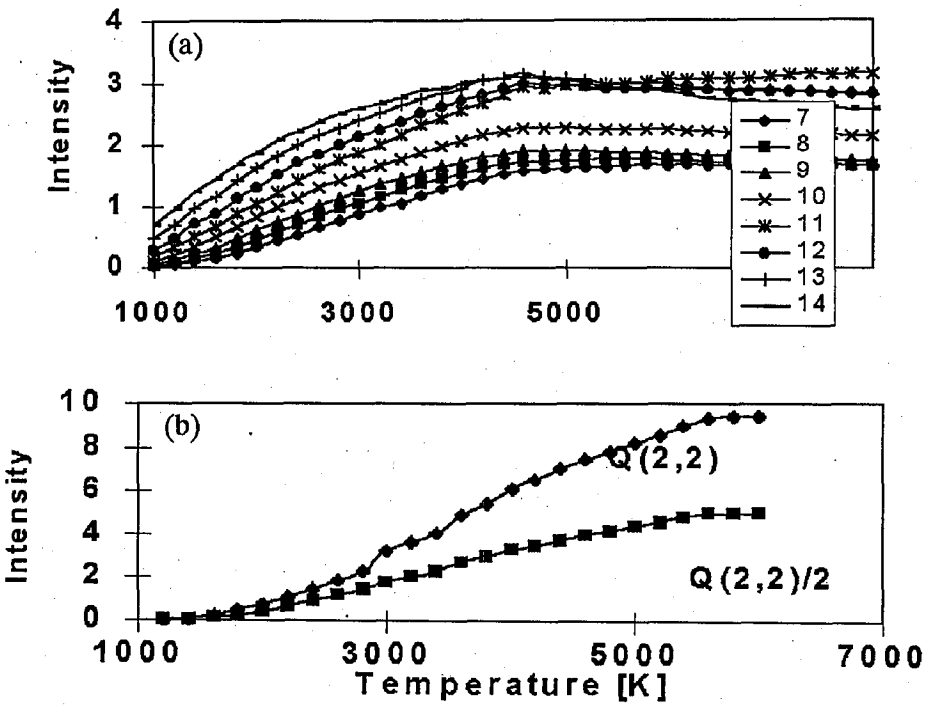


Fig. 4. Evolution of the integrated intensities of the thermometric lines as a function of the temperatures $T_R$ (a) and $T_V$ (b).

TABLE II

Polynomial curve fit coefficients for the thermometric functions as a function of temperature.

| | Degree | | | |
|---|---|---|---|---|
| Line | 0 | 1 | 2 | 3 |
| 6 | 1033.73 | 5381.49 | −5593.99 | 2701.53 |
| 7 | 1010.75 | 3679.22 | −2605.80 | 1118.71 |
| 8 | 921.81 | 3187.19 | −2135.97 | 908.71 |
| 9 | 814.42 | 2871.26 | −1896.04 | 775.97 |
| 10 | 744.37 | 2217.11 | −1151.10 | 417.49 |
| 11 | 753.62 | 1384.74 | −286.71 | 95.83 |
| 12 | 565.45 | 1531.88 | −561.93 | 174.51 |
| 13 | 426.70 | 1440.87 | −530.85 | 162.16 |
| 14 | −728.96 | 3561.30 | −1982.99 | 449.12 |
| Q(2,2) | 305.98 | 1475.96 | −354.22 | 47.58 |
| Q(2,2)/2 | 332.32 | 857.60 | −120.89 | 8.58 |

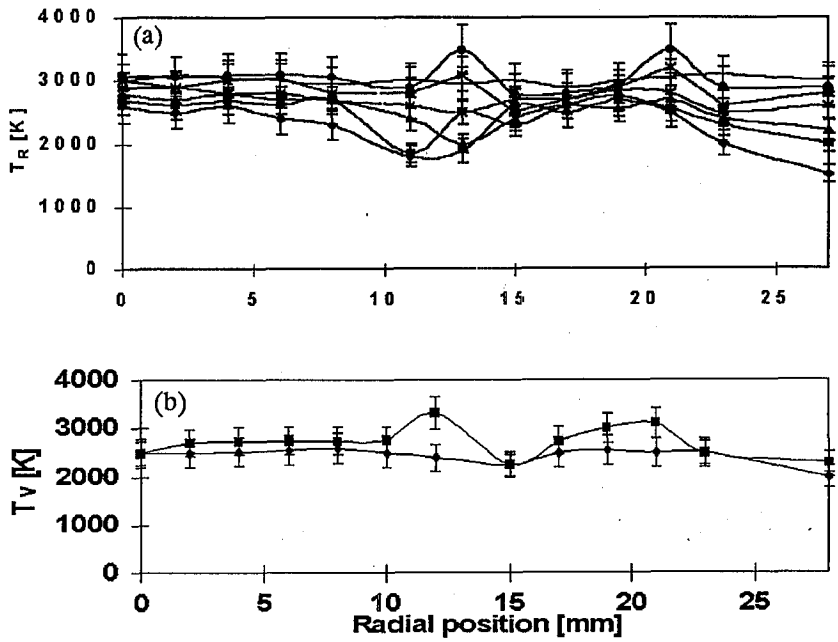


Fig. 5. Rotational (a) and vibrational (b) temperatures ($T_R$ and $T_V$) as a function of the radial position, after Abel inversion of the lateral data. Until 10 mm, $T_R$ and $T_V$ are constants, after 12 mm the results fluctuate and show a decreasing trend. Settings: [Ar] = 100 scc/s, [$CH_4$] = 4.44 scc/s, $p$ = 100 Pa, $I_{arc}$ = 50 A.

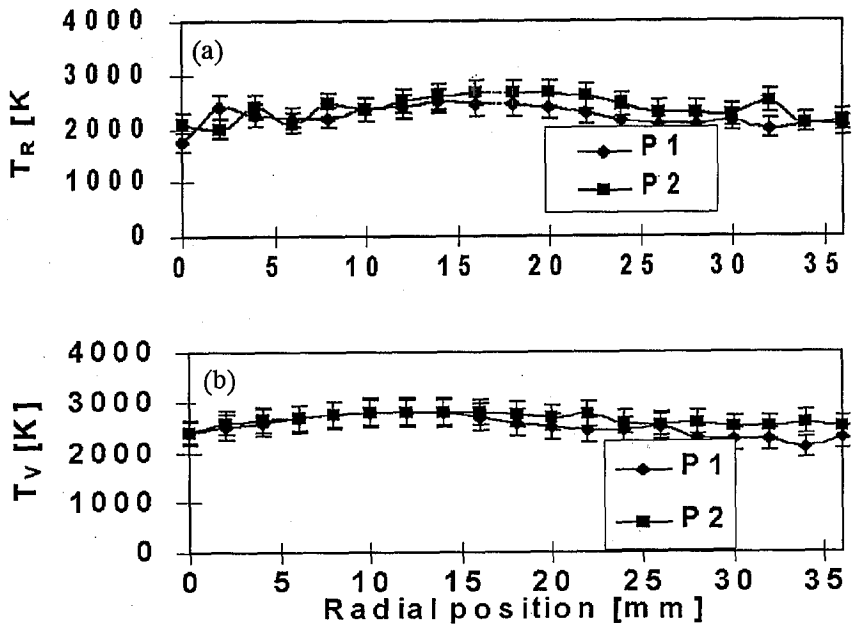


Fig. 6. Rotational temperature $T_R$ (a) and vibrational temperature $T_V$ (b) as a function of radial position, before Abel inversion of the lateral data. Settings: [Ar] = 100 scc/s, $[CH_4]$ = 4.44 scc/s, $p$ = 100 Pa, $I_{arc}$ = 50 A. Axial position: +20 mm, $\Delta$: 60 mm.

The rotational temperatures are calculated using the evolution of the thermometric lines as a function of temperature, as shown in Fig. 4. In such a way, we obtain the so-called thermometric functions which are integrated intensities of line-like transitions composed of several rotational transitions. The procedure for the temperature calculations of $T_V$ and $T_R$ are fully automated. Thus only the integrated intensities are needed to calculate the temperatures with a simple program. The coefficients of the polynomial curves of the thermometric functions are given in Table II. In Figs. 5, 6 and 7 the results are summarised for $T_V$ and $T_R$, with and without Abel inversion of the lateral data, and as a function of radial and axial position. All thermometric functions are used. For the determination of $T_V$ one of the curves corresponds to the full Q(2,2) integrated intensity while the other one represents the violet half part of the integrated Q(2,2) intensity. Using the violet half part of the Q(2,2) head avoids possible errors introduced by the complex composition of the red $P$ branch overlapping the system.

## 4. Discussion and conclusion

Neglecting the lambda doubling in the $A^2\Delta$ state and the predissociation do not influence the quality of the calculations of the relative intensities. The

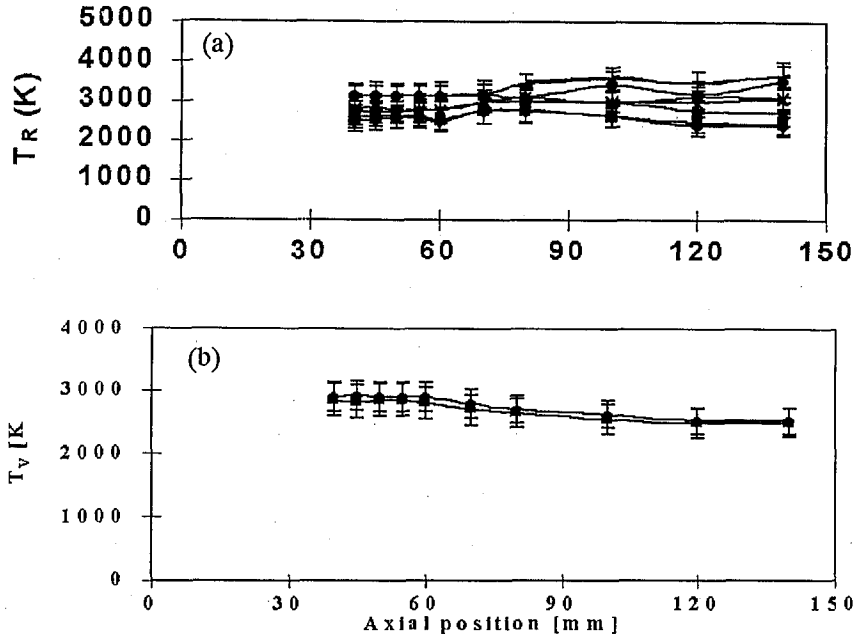


Fig. 7. Rotational temperatures $T_R$ (a) and vibrational temperatures $T_V$ (b) as a function of axial position, before Abel inversion. [Ar] = 100 scc/s, [$CH_4$] = 4.44 scc/s, $p = 100$ Pa, $I_{arc} = 50$ A.

simulation of the molecular spectra is done in the intermediate Hund case (a) and (b) with the assumption of the thermal equilibrium.

The choice of the red and violet limits of the thermometric lines as well as the continuum background need a careful attention. The result obtained by the Boltzmann method, which gives rotational temperatures of 2900–3500 K for different axial and radial positions, shows the Boltzmann distribution of rotational levels. The results obtained by the thermometric method show a small deviation from the equilibrium between the vibrational and rotational temperatures. The vibrational temperature is assumed to be close to the electron temperature and the rotational temperature equals the gas temperature. The temperature obtained by the two methods, the "Boltzmann" method and the "thermometer" method, are similar, justifying the proposed diagnostics method of the thermometric functions. When the measurements are done near the nozzle exit in the supersonic region of the plasma jet the CH emission are expected to come mainly from the edge of the plasma. Therefore, for a more reliable diagnostic along the flow, it is necessary to Abel-invert the experimental data before further processing.

We conclude that the method of thermometric functions for the determination of $T_R$ and $T_V$ is accurate and convenient because no complex high

resolution optical system is required. It is therefore also applicable in industrial conditions.

## Acknowledgment

This work is a part of the research program of the Stiching Fundamentateel Oderzoek der Materie (FOM).

## References

[1] A. Czernichowski, A. Ranaivosoloarimanana, *Chemtech* **26**, 45 (1996).

[2] J.J. Beulens, A.J.M. Buuron, D.C. Schram, *Surf. Coat. Technol.* **47**, 401 (1991).

[3] G.M.W. Kroesen, C.J. Timmermans, D.C. Schram, *Pure Appl. Chem.* **60**, 795 (1986).

[4] A. Czernichowski, P. Czernichowski, A. Ranaivosoloarimanana, in: *11th World Hydrogen Energy Conf., Stuttgart, 1996*, Eds. T.N. Veziroglu, C.-J. Winter, J.P. Baselt, G. Kreysa, Schön & Wedzel GmbH, Frankfurt/M, p. 661.

[5] C.J. Timmermans, G.M.W. Kroesen, P.M. Vallinga, D.C. Schram, *Z. Naturfosch. A* **43**, 806 (1986).

[6] J.J. Beulens, A.J.M. Buuron, T.H.J. Bisschops, A.B.M. Hüsken, *J. Phys. (France)* **51**, C5 (1990).

[7] J.J. Beulens, Ph.D. Thesis, Eindhoven Univ. of Techn., The Netherlands (1992).

[8] I. Kovacs, *Rotational Structure in the Spectra of Diatomic Molecules*, Adam Hilger, London 1969.

[9] J. Koulidiati, J.J. Beulens, A. Czernichowski, D.C. Schram, *J. Phys. (France)* **51**, C5-297 (1990).

[10] G. Phillips, *J. Mol. Spectrosc.* **28**, 223 (1968).

[11] G. Herzberg, *The Spectra and Structure of Simple Free Radicals*, Cornel University Press, Ithaca 1971.

[12] G. Herzberg, *Molecular Spectra and Molecular Structure*, part IV: *Constant of Diatomic Molecules*, Van Nostrand, Princeton 1979.

[13] J. Koulidiati, Ph.D. Thesis, Université d'Orléans, France 1991.

[14] E. Fagerhölm, *Ark. Mat. Astro. Fys. A* **27**, No. 19 (1940).

[15] L. Gerö, *Z. Phys.* **118**, 27 (1941).

[16] Z. Bembenek, R. Kepa, A. Para, M. Rytel, M. Zachwieja, *J. Mol. Spectrosc.* **139**, 1 (1990).